Temperature Distributions in Supersonic Turbulent Boundary Layers

H. U. MEIER* AND J. C. ROTTA†
Deutsche Forschungs- und Versuchsanstalt für Luft- und Raumfahrt, Aerodynamische Versuchsanstalt, Göttingen, Germany

Experimental investigations of total temperature and Mach number distributions in turbulent boundary layers have been performed in the Mach number range from 1.75 to 4.5, using a newly developed combined temperature and pressure probe. The measurements carried out so far have been used to reanalyze the process of heat transport by calculating the turbulent Prandtl number distribution throughout the boundary layer. The results show an increase of the turbulent Prandtl number close to the surface, thus indicating that the turbulent transport of heat decreases more rapidly towards the wall than the turbulent transport of momentum. A simple relation, based on the Prandtl mixing length theory, is proposed for the variation of the turbulent Prandtl number within the viscous layer. This relation gives temperature distributions that are in good agreement with the experimental data in the region of constant shear stress.

Nomenclature

a = speed of sound
A = van Driest's constant, Eq. (41)
A_q = const, as defined by Eq. (42)
c_p = specific heat at constant pressure
c_f = skin friction coefficient, $c_f = 2\tau_W/(\rho U^2)_\infty$
l = Prandtl's mixing length, Eq. (41)
l_q = mixing length for heat transport, Eq. (42)
M = Mach number, $M = U/a$
M_τ = Mach number parameter, $M_\tau = (c_f/2)^{1/2}M_\infty$
p = static pressure
p_0 = total pressure
Pr = molecular Prandtl number, $Pr = \mu c_p/\lambda$
Pr_t = turbulent Prandtl number, Eq. (16)
q = heat flux (in the y direction)
r = boundary-layer recovery factor
r_p = recovery factor of the probe, Eq. (2)
Re/cm = Reynolds number, based on freestream values and the length of 1 cm
Re_2 = Reynolds number, based on freestream values and the momentum thickness, $Re_2 = U_\infty\delta_2/\nu_\infty$
T = static temperature
T_B = reference temperature of the probe thermocouple, $T_B = T_{0\infty}$
T_0 = total temperature
T_e = equilibrium temperature, $T_e = T_\infty[1 + r(\gamma - 1)M_\infty^2/2]$
T' = temperature fluctuations
U,V = mean velocity components
u,v = components of velocity fluctuations
u_τ = shear stress velocity, $u_\tau = (\tau_W/\rho_W)^{1/2}$
x,y = Cartesian coordinates
y^* = dimensionless wall distance, $y^* = yu_\tau/\nu_W$
β_q = heat flux parameter, $\beta_q = q_W/(c_pT_W\rho_W u_\tau)$
γ = ratio of specific heats
δ = boundary-layer thickness
δ_2 = momentum thickness,

$$\delta_2 = \int_0^\delta \rho U/(\rho U)_\infty(1 - U/U_\infty)dy$$

ϵ_q = eddy heat conductivity
ϵ_τ = eddy viscosity
κ = von Kármán constant
κ_q = const, as defined by Eq. (42)
λ = thermal conductivity
μ = dynamic viscosity
ν = kinematic viscosity
ρ = density
ρ' = density fluctuation
τ = shear stress

Subscripts

m = value, measured with boundary-layer probe (measured value)
w = conditions at the wall
∞ = value in the freestream

1. Introduction

THE knowledge of the total temperature distribution in turbulent supersonic boundary layers is necessary for the estimation of the skin friction and heat-transfer coefficients of modern flight vehicles. Theoretical calculations of the temperature profile are usually based on the so called "Crocco solution," which includes assumptions not compatible with real flow conditions. On the other hand, there is a considerable amount of variation in the temperature distributions calculated from measurements made by different experimenters. These measured temperature distributions are not in satisfactory agreement with existing theoretical results.[1] Furthermore, it is difficult to ascertain what portion of the variation results from differences in the boundary layers, e.g., "history effects," and what portion is caused by shortcomings of the test methods or techniques. Therefore, further experiments should be made in order to clarify the observed discrepancies.

In the present study, measurements were made at nearly adiabatic wall conditions on a flat plate and on a flat nozzle wall in two separate wind tunnels. However, the same combined total temperature and total pressure probe was used in both tunnels to obtain the data.[2] An analysis of the heat transport process in turbulent compressible boundary layers is made, based on these measurements.

2. Experiments

The experimental work on compressible turbulent boundary layers, performed in two different tunnels, is briefly described

Presented as Paper 70-744 at the AIAA 3rd Fluid and Plasma Dynamics Conference, Los Angeles, Calif., June 29–July 1, 1970; submitted August 24, 1970; revision received March 16, 1971. It is acknowledged that the measurements on the flat plate in the (3 × 4 ft) High Supersonic Wind Tunnel of the Royal Aircraft Establishment, Bedford, England, were performed with D. G. Mabey and W. G. Sawyer as a joint work of England and Germany.

* Staff member. Member AIAA.
† Staff member.

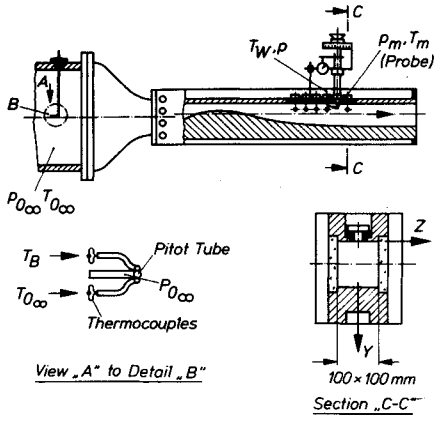

Fig. 1 Test arrangement in the "Small Supersonic Wind Tunnel" of the AVA.

as follows:

1) Measurements on a flat plate were made in the 3 × 4 ft "High Supersonic Wind Tunnel (HSST)" of the Royal Aircraft Establishment (RAE), Bedford, England. A detailed description of the tunnel and the flat plate is given in Ref. 3. The plate was 1664 mm long and 890 mm wide and was supported by two cantilevers bolted to the side walls in a fixed position. The leading-edge wedge angle was 10° and its bluntness deliberately made rather large (0.25 mm) to avoid variations in bluntness caused by the sandblasting during the prolonged period of tests. The bottom surface and the supporting cantilevers were thermally insulated to approximate adiabatic flow conditions as much as possible. Nevertheless, the measured recovery temperatures on the flat surface of the plate were generally about 22°C, considerably higher than the theoretical equilibrium temperature of about 15°C [$r = (Pr)^{1/3} = 0.89$].

In this paper, only measurements are discussed that were performed at a fixed position from the leading edge (x_{LE} = 870 mm). The Reynolds numbers were varied by changing the settling chamber pressure. The detailed description of the test arrangement, including the data of four other positions from the leading edge, is given in Ref. 4.

2) The measurements in the "Small Supersonic Wind Tunnel" of the AVA (Aerodynamische Versuchsanstalt), Göttingen, were performed on a flat nozzle wall. This tunnel, with a test section of 10 × 10 cm, is described in Ref. 5. The total pressure and total temperature profiles were measured at six different distances from the nozzle throat at nearly adiabatic wall conditions. These conditions were obtained by heating the air in the wind tunnel up to a temperature at which the measured wall temperature was equal to the ambient temperature. The influence of Reynolds number variation at constant Mach number was not investigated in these tests.

The general range of test conditions in the two wind tunnels is summarized in Table 1. The investigations in both tunnels were performed with the combined total temperature and pressure probe,[2] which was developed in the Small Supersonic

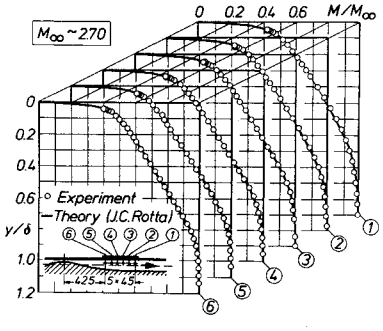

Fig. 2 Mach number profiles on the flat nozzle wall.

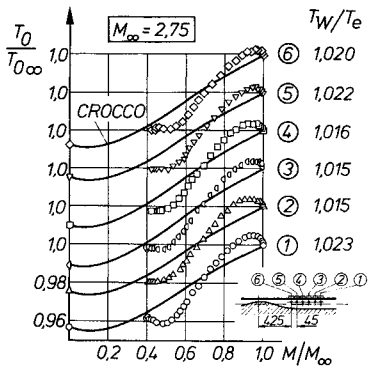

Fig. 3 Total temperature profiles on the flat nozzle wall.

Wind Tunnel of the AVA. This device results from an attempt to avoid most of the disadvantages of existing shielded total temperature probes. To obtain high sensitivity, the temperature difference between the probe and the reference thermocouple, which is installed in the settling chamber, is directly indicated. The accuracy in temperature measurement of the probe and the electronic equipment is ±0.1°C. The electronic equipment and the general arrangement of the tests in the HSST of the RAE and the Small Supersonic Wind Tunnel of the AVA are very similar. The arrangement of the tests in the AVA tunnel is shown in Fig. 1.

3. Data Reduction

The Mach number profiles were calculated in the usual manner from the measured pressure distributions in the boundary layer.[5] For pressure ratios of $p/p_0 \geq 0.528$ the Mach number was evaluated from the Bernoulli equation for compressible flow. For supercritical pressure ratios $p/p_0 \leq 0.528$ the Rayleigh Pitot formula was used. The assumption of a constant static pressure through the boundary layer is made. The static pressure p was measured at the wall for AVA investigations, while it was calculated from the ratio of settling chamber pressure to Pitot pressure for the RAE data reduction.

The ratio of local total to static temperature is given by

$$T_0/T = 1 + [(\gamma - 1)/2]M^2 \tag{1}$$

It could be shown in Ref. 2 that the calibration factor of the probe, defined as

$$r_p = (T_m - T)/(T_0 - T) \tag{2}$$

is mainly dependent on the mass rate of flow $\dot{m}$ which passes the thermocouple. Since in these measurements the mass flow changed during the boundary-layer traverse, the calibration factor of the probe was not constant. Therefore with each change of probe position in the boundary layer the exhausted mass flow rate was measured. The calibration of the probe for variable mass flow was obtained outside of the boundary layer after each traverse. With Eqs. (1) and (2) the local total temperature can be obtained as a function of the measured total temperature T_m and the probe calibration factor r_p. This relationship is

$$T_0 = T_m/[r_p + (1 - r_p)/\{1 + [(\gamma - 1)/2]M^2\}] \tag{3}$$

The velocity ratio at any point can be expressed as a function of Mach number and total temperature, as follows

$$\frac{U}{U_\infty} = \frac{M}{M_\infty}\left\{\frac{1 + [(\gamma - 1)/2]M_\infty^2}{1 + [(\gamma - 1)/2]M^2}\,\frac{T_0}{T_{0\infty}}\right\}^{1/2} \tag{4}$$

Likewise, by using the ideal gas equation of state and constant static pressure, the density ratio can be calculated as a function of the measured variables from

$$\frac{\rho}{\rho_\infty} = \frac{1 + [(\gamma - 1)/2]M^2}{1 + [(\gamma - 1)/2]M_\infty^2}\,\frac{T_{0\infty}}{T_0} \tag{5}$$

All of the desired boundary-layer properties have now been expressed as a function of the measured variables.

Table 1 Test conditions

Tunnel	Size of test section, cm	M_∞	$Re/\text{cm}\cdot 10^{-5}$	$Re_2\cdot 10^{-4}$
RAE	91.5×122	$2.5 - 4.5$	$1.1 - 3.0$	$0.9 - 2.0$
AVA	10×10	$1.5 - 3.0$	$1.4 - 0.8$	$0.4 - 1.0$

4. Results and Discussion of Measurements

To determine the local skin friction coefficients from the measured boundary-layer profiles, analytical velocity profiles are constructed from the law of the wall for compressible flow, in accordance with Ref. 6, and Coles' wake function. An additional distribution is introduced in order to eliminate the abrupt change in the slope $\partial U/\partial y$ at the outer edge. The main point is that, for given conditions, the boundary-layer profile is fully determined when values of wall shear stress τ_W and boundary-layer thickness δ are known. Now, an iterative calculation procedure has been used to determine τ_W and δ in such a way that the calculated profile is in best agreement with the experimental one. This is accomplished by requiring that the root-mean-square deviation between measured and calculated profiles becomes a minimum. A more detailed description of this procedure is given in Ref. 7.

The Mach number profiles measured at six different stations on the plane nozzle wall are shown in Fig. 2. All profiles are in excellent agreement with the profiles calculated by the method just described. Figure 2, in which the Mach number distributions are presented perspectively, gives no unequivocal information about the similarity of the profiles. However, the wake factor of the Coles' wake function increases with increasing distance from the nozzle throat. This indicates less full profiles farther downstream.

The corresponding total temperature profiles are shown in Fig. 3. The ratio of local and freestream total temperature $T_0/T_{0\infty}$ is plotted against the Mach number ratio M/M_∞. Crocco's relation

$$\frac{T}{T_\infty} = \frac{T_W}{T_\infty} + \frac{T_e - T_W}{T_\infty}\left(\frac{U}{U_\infty}\right) - r\,\frac{\gamma - 1}{2}\,M_\infty^2\left(\frac{U}{U_\infty}\right)^2 \quad (6)$$

is shown for comparison, assuming a recovery factor, $r = 0.89$.‡ Systematic deviations between the Crocco distribution and the measured values are observed. Firstly, the experimental total temperature distribution decreases as the wall is approached and then increases again. Secondly, the so-called overshoot in the outer part of the boundary layer increases with increasing distances. This overshoot should be constant in accordance with the total energy balance for a thermally insulated flat surface. The change in the overshoot may be explained by the fact that the heat flux from the fluid to the surface is not constant on the plane nozzle wall. The Mach number M_∞ is increasing from the nozzle throat ($M_\infty = 1$) to the test section. Consequently, the equilibrium temperature T_e is decreasing. Since the ambient temperature is constant, there must be a greater heat flux through the wall near the throat than in the test section, where the measured wall temperature T_W is very close to the equilibrium temperature T_e. Thus, full similarity could not be established with these investigations.

The results obtained from measurements on the flat plate at a freestream Mach number $M_\infty = 4.5$ are shown in Figs. 4 and 5. The Mach number profiles, plotted as M/M_τ against

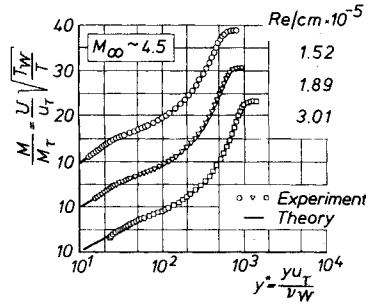

Fig. 4 Mach number profiles on the flat plate.

the dimensionless wall distance $y^* = u_\tau y/\nu_W$, are very close to the calculated profiles. $M_\tau = (c_f/2)^{1/2}M_\infty$ is the Mach number parameter, $u_\tau = (\tau_W/\rho_W)^{1/2}$ the shear stress velocity. The corresponding total temperature profiles (Fig. 5) show very different shapes for the outer parts compared with those measured on the nozzle wall. At the moment, no explanation can be offered for the vanishing of the overshoot. Near the surface the temperature distribution of the two experiments agree with each other.

5. Turbulent Prandtl Numbers

The measurements show that the total temperature decreases as the wall is approached and then increases again. To explain this behavior, further information regarding the turbulent mechanism in this region seems necessary. In order to calculate the turbulent Prandtl numbers in the boundary layer, the shear stress and heat flux distributions must be estimated first.

If the usual boundary-layer approximations are accepted (see H. Schlichting,[8] Chap. 23a), and the mass flux in y direction is defined by

$$\langle \rho V \rangle = \rho V + \langle \rho' v \rangle \quad (7)$$

then the equations for continuity, momentum and energy for two-dimensional flow without pressure gradients read as follows:

$$\partial(\rho U)/\partial x + \partial(\langle \rho V \rangle)/\partial y = 0 \quad (8)$$

$$\frac{\partial(\rho U^2)}{\partial x} + \frac{\partial(\langle \rho V \rangle U)}{\partial y} = \frac{\partial \tau}{\partial y} = \frac{\partial(\tau_l + \tau_t)}{\partial y} \quad (9)$$

$$c_p\left[\frac{\partial(\rho U T_0)}{\partial x} + \frac{\partial(\langle \rho V \rangle T_0)}{\partial y}\right] - \frac{\partial(U\tau)}{\partial y} = \frac{\partial q}{\partial y} = \frac{\partial(q_l + q_t)}{\partial y} \quad (10)$$

The contribution of molecular friction is

$$\tau_l = \mu \partial U/\partial y \quad (11)$$

and the apparent shear stress may be expressed in terms of the Boussinesq relation

$$\tau_t = -\rho\langle uv \rangle = \rho \epsilon_\tau \partial U/\partial y \quad (12)$$

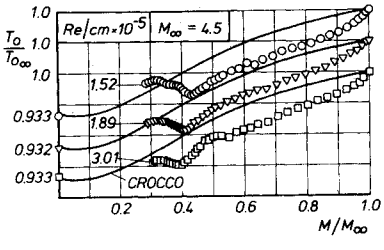

Fig. 5 Total temperature profiles on the flat plate.

‡ The familiar presentation of the data in terms of $(T_o - T_W)/(T_{o\infty} - T_W)$ vs U/U_∞ was not used here, because the deviations from Crocco's formula would appear unduly enlarged due to the small difference $T_{o\infty} - T_W$. The Mach number M was preferred to the velocity U since M is determined from the pressure measurements alone, independently of the temperature measurements. Thus, Figs. 3 and 5 show temperature measurements vs pressure measurements.

Similarly, the molecular contribution to the heat flux is

$$q_l = \lambda \partial T/\partial y \tag{13}$$

and the apparent heat flux can be written as

$$q_t = -c_p \rho \langle vT' \rangle = c_p \rho \epsilon_q \partial T/\partial y \tag{14}$$

In the Eqs. (7) to (14) the values of ρ, U, V, T, τ, and q are averaged values with respect to time, and $\langle \rho' v \rangle$, $\langle uv \rangle$, $\langle vT' \rangle$ are the time averaged products of fluctuating quantities. ϵ_q and ϵ_τ are the eddy heat conductivity and eddy kinematic viscosity, respectively.

For laminar flow, the momentum and thermal transport mechanisms are related to each other by the molecular Prandtl number $Pr = \mu c_p/\lambda$. Similarly, the turbulent Prandtl number is defined as

$$Pr_t = \epsilon_\tau/\epsilon_q \tag{15}$$

With the definitions of Eqs. (11–14) the turbulent Prandtl number can be expressed as

$$Pr_t = c_p(\tau - \tau_l)/(q - q_l)(\partial T/\partial y)/(\partial U/\partial y) \tag{16}$$

The specific heat at constant pressure c_p, and the molecular Prandtl number Pr are constant, while the density ρ and the dynamic viscosity μ are functions of the static temperature T. The local values of the shear stress τ, the heat flux q, the derivatives $\partial T/\partial y$ and $\partial U/\partial y$ can be calculated from measurements.

A. Calculation of Shear Stress and Heat Flux Profiles

After substituting Eq. (8) into Eqs. (9) and (10), the integration with respect to y of the thermal energy and momentum equations yields

$$\tau = \int_0^y \frac{\partial(\rho U^2)}{\partial x}\, d\tilde{y} - U \int_0^y \frac{\partial(\rho U)}{\partial x}\, d\tilde{y} + C_1 \tag{17}$$

$$q = c_p \left[\int_0^y \frac{\partial(\rho U T_0)}{\partial x}\, d\tilde{y} - T_0 \int_0^y \frac{\partial(\rho U)}{\partial x}\, d\tilde{y} \right] - U\tau + C_2 \tag{18}$$

The constants C_1 and C_2 in Eqs. (17) and (18) are determined by the boundary conditions $y = \delta$: $\tau = q = 0$.

There are not enough data to differentiate the field quantities with respect to x. Therefore, selfsimilar boundary-layer profiles are assumed, although the similarity is not fully established. If the velocity and temperature profiles in x direction are selfsimilar, the partial differential quotient $\partial(\rho U)/\partial x$ in Eqs. (17) and (18) follows from the assumption $\rho U = \rho_\infty U_\infty F(\zeta)$, which implies that $\rho U/(\rho U)_\infty$ is only a function of the dimensionless wall distance $\zeta = y/\delta$. After the partial differentiation with respect to x, followed by a partial integration with respect to y, one gets in a dimensionless form

$$\frac{1}{\rho_\infty U_\infty} \int_0^y \frac{\partial(\rho U)}{\partial x}\, d\tilde{y} = -\frac{1}{\delta}\frac{d\delta}{dx} \left[\frac{\rho U}{\rho_\infty U_\infty} y - \int_0^y \frac{\rho U}{\rho_\infty U_\infty}\, d\tilde{y} \right] \tag{19}$$

The integration of the other partial differential quotients $\partial/\partial x$ in Eqs. (17) and (18), with similar assumptions, gives the following results:

$$\frac{1}{\rho_\infty U_\infty} \int_0^y \frac{\partial(\rho U^2)}{\partial x}\, d\tilde{y} = -\frac{1}{\delta}\frac{d\delta}{dx} \left[\frac{\rho}{\rho_\infty} \left(\frac{U}{U_\infty}\right)^2 y - \int_0^y \frac{\rho}{\rho_\infty} \left(\frac{U}{U_\infty}\right)^2 d\tilde{y} \right] \tag{20}$$

$$\frac{1}{(\rho U T)_\infty} \int_0^y \frac{\partial(\rho U T_0)}{\partial x}\, d\tilde{y} = -\frac{1}{\delta}\frac{d\delta}{dx} \left[\frac{\rho U T_0}{\rho_\infty U_\infty T_\infty} y - \int_0^y \frac{\rho U T_0}{\rho_\infty U_\infty T_\infty}\, d\tilde{y} \right] \tag{21}$$

In these equations, the gradient $d\delta/dx$ describes the growth of the boundary layer in x direction. With the local skin friction coefficient c_f known, the von Kármán momentum equation can be used in the form

$$(1/\delta)(d\delta/dx) = (1/\delta_2)(d\delta_2/dx) = c_f/2\delta_2 \tag{22}$$

which also implies similarity of the profiles. Introducing all the expressions of Eqs. (19–22) into the Eqs. (17) and (18), one obtains, for the shear stress and heat flux distributions, the relations

$$\frac{\tau}{\rho_\infty U_\infty^2} = -\frac{c_f}{2\delta_2} \left[\frac{U}{U_\infty} \int_0^y \frac{\rho U}{\rho_\infty U_\infty}\, d\tilde{y} - \int_0^y \frac{\rho U^2}{\rho_\infty U_\infty^2}\, d\tilde{y} \right] + C_1 \tag{23}$$

$$\frac{q}{c_p(\rho U T)_\infty} = \frac{c_f}{2\delta_2} \left[\frac{T_0}{T_\infty} \int_0^y \frac{\rho U}{\rho_\infty U_\infty}\, d\tilde{y} - \int_0^y \frac{\rho U T_0}{(\rho U T)_\infty}\, d\tilde{y} \right] - \frac{U}{U_\infty}\frac{\tau}{\rho_\infty U_\infty^2}(\gamma - 1)M_\infty^2 + C_2 \tag{24}$$

The supposition of similarity is not fully satisfied by the total temperature profiles. This has the consequence that Eq. (24) gives incorrect heat flux distributions, especially close to the surface. For this reason, a factor C_3 has been introduced, such that Eq. (21) takes the form

$$\frac{1}{(\rho U T)_\infty} \int_0^y \frac{\partial(\rho U T_0)}{\partial x}\, d\tilde{y} = -C_3 \frac{c_f}{2\delta_2} \left[\frac{\rho U T_0}{(\rho U T)_\infty} y - \int_0^y \frac{\rho U T_0}{(\rho U T)_\infty}\, d\tilde{y} \right] \tag{25}$$

Substituting Eq. (25) in Eq. (18) one finds the local heat flux to be

$$\frac{q}{c_p(\rho U T)_\infty} = -C_3 \frac{c_f}{2\delta_2} \left[\frac{\rho U T_0}{(\rho U T)_\infty} y - \int_0^y \frac{\rho U T_0}{(\rho U T)_\infty}\, d\tilde{y} \right] + \frac{c_f}{2\delta_2} \left[\frac{\rho U T_0}{(\rho U T)_\infty} y - \frac{T_0}{T_\infty} \int_0^y \frac{\rho U}{\rho_\infty U_\infty}\, d\tilde{y} \right] - \frac{U}{U_\infty}\frac{\tau}{\rho_\infty U_\infty^2}(\gamma - 1)M_\infty^2 + C_2 \tag{26}$$

where the correction factor C_3 and the integration constant C_2 are determined by the boundary conditions 1) $y = \delta$: $q = 0$, 2) $y = 0$: $q_W/[c_p(\rho U T)_\infty] = C_2$. This means, by proper choice of C_3, the heat flux distribution can be adjusted to the correct value at the wall.

For an adiabatic wall, it follows from boundary condition 2 that $q_W/[c_p(\rho U T)_\infty] = C_2 = 0$.

In the case of heat transfer from the flow to the surface, we get from Newton's friction law and Fourier's heat conduction law the relation

$$q_W = \tau_W c_p/Pr(\partial T/\partial U)_W \tag{27}$$

If the derivative $(\partial T/\partial U)_W$ is to be determined from measurements, one obtains with the boundary conditions $y = 0$: $M = 0$ and $T = T_0 = T_W$ the expression

$$(\partial T/\partial U)_W = [\partial(T/T_\infty)/\partial(M/M_\infty)]_W (T_\infty/T_W)^{1/2} T_\infty/U_\infty \tag{28}$$

However, $(\partial T/\partial M)_W$ cannot be determined with great accuracy, since no measurements can be made in the viscous sublayer. Thus, an assumption, similar to that in the Crocco equation has been applied: the local static temperature T_{ad} in the boundary layer on an adiabatic flat surface may be given as $T_{ad} = T_\infty F(y/\delta)$. Then small deviations from these adiabatic flow conditions can be taken into account using the approximation $T = T_{ad} + (U/U_\infty)a_1 + a_2$. The constants a_1 and a_2 are obtained from the boundary conditions $y = 0$: $T = T_W$, $T_{ad} = T_e$, $y = \delta$: $T = T_\infty$, $T_{ad} = T_\infty$, such that one

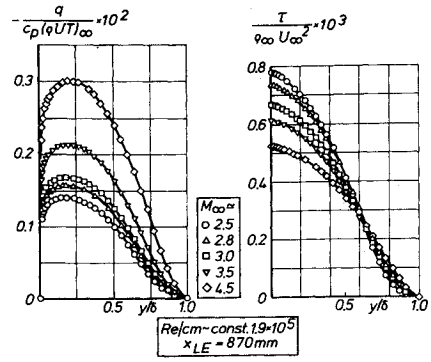

Fig. 6 Heat flux and shear stress distributions on the flat plate for different Mach numbers.

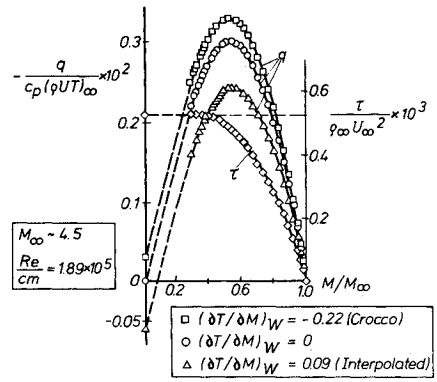

Fig. 8 Heat flux and shear stress distributions using different values of $(\partial T/\partial M)_W$.

obtains $T = T_{ad} + (T_W - T_e)[1 - (U/U_\infty)]$. Because of $(\partial T_{ad}/\partial y)_W = 0$, the derivative $(\partial T/\partial U)_W$ takes the form

$$(\partial T/\partial U)_W = (T_e - T_W)/U_\infty \tag{29}$$

Examples of calculated shear stress and heat flux distributions are given in Figs. 6–8. With increasing Mach numbers the local skin friction coefficient decreases, and so does the local shear stress, as shown in Fig. 6. Also shown in this figure are the corresponding heat flux distributions, assuming adiabatic wall conditions. For constant freestream Reynolds numbers, the total temperature was regulated in such a manner as to give constant wall temperatures at all Mach numbers. Consequently one obtains larger local heat flux with increasing Mach number.

The effect of Reynolds number variation with respect to the shear stress and heat flux distributions in the boundary layer is shown in Fig. 7. If the Reynolds number was decreased by lowering the settling chamber pressure for a constant Mach number, the local values of the heat fluxes and shear stresses increase, due to the fact that close to the wall the viscosity becomes greater.

In Fig. 8 it is demonstrated that the accuracy of the calculated heat flux distributions is sensitive to changes in the derivative $(\partial T/\partial U)_W$, which fixes the integration constant C_2 in Eq. (26). Linear interpolation between the wall temperature T_W and the closest measured point results in a positive derivative $(\partial T/\partial U)_W$, which is probably not compatible with the test conditions. The estimation of this derivative, using the Crocco-type solution of Eq. (29), predicts a small rate of heat transfer from the plate to the flow.

B. Determination of the Local Temperature- and Velocity Derivatives $\partial T/\partial y$ and $\partial U/\partial y$

The calculation of turbulent Prandtl numbers from low-speed heat transfer tests suffers from the poor accuracy, with which $(\partial T/\partial y)/(\partial U/\partial y)$ is determined from the experimental data. In order to minimize the errors, the following procedure has been applied in the present case. The actual value of the static temperature close to the wall is strongly affected by the Mach number, whereas the total temperature shows only small alterations. For this reason, the total temperature and Mach-number distributions have been used to determine the derivatives $\partial T/\partial y$ and $\partial U/\partial y$.

From the ratio of the static temperatures

$$T/T_\infty = (T_0/T_\infty)/\{1 + [(\gamma - 1)/2]M^2\} \tag{30}$$

one obtains, by differentiation with respect to M,

$$\frac{\partial(T/T_\infty)}{\partial M} = \frac{[\partial(T_0/T_\infty)/\partial M] - (\gamma - 1)(T/T_\infty)M}{1 + [(\gamma - 1)/2]M^2} \tag{31}$$

and in a similar way

$$\frac{(\partial U/U_\infty)}{\partial M} = \frac{(T/T_\infty)^{1/2}}{M_\infty} + \frac{1}{2}\frac{M}{M_\infty}\left(\frac{T_\infty}{T}\right)^{1/2}\frac{\partial(T/T_\infty)}{\partial M} \tag{32}$$

Consequently, one finds

$$(\partial T/\partial y)/(\partial U/\partial y) = [\partial(T/T_\infty)/\partial M][\partial M/\partial(U/U_\infty)] \tag{33}$$

This expression includes only the variables T_0 and M, and requires no differentiation with respect to y. Differentiation with respect to y is necessary to determine the molecular contributions τ_l and q_l, which are only small correction terms in Eq. (16). The measured total temperature and Mach number distribution were first smoothed and then differentiated. Quite accurate results are achieved in this way.

C. Distribution of Turbulent Prandtl Numbers

When the ratio of the local derivatives $(\partial T/\partial y)/(\partial U/\partial y)$, as well as the local values of the shear stress τ, and heat flux q, are calculated, one can obtain the turbulent Prandtl numbers using Eq. (16). In Fig. 9 the turbulent Prandtl number distributions, calculated from the total pressure and temperature profiles of the flat plate, are plotted vs the dimensionless distance y^*. For all the investigated Mach numbers the

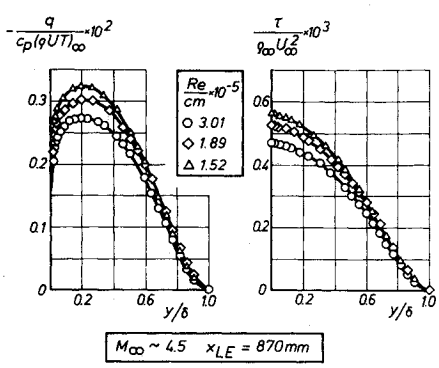

Fig. 7 Heat flux and shear stress distributions on the flat plate for different Reynolds numbers.

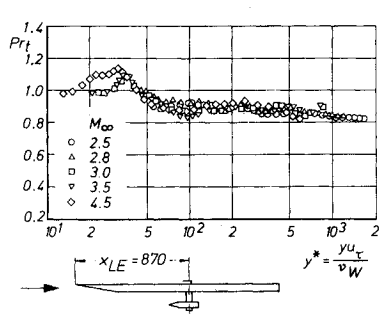

Fig. 9 Turbulent Prandtl numbers Pr_t vs dimensionless wall distance y^* on a flat plate.

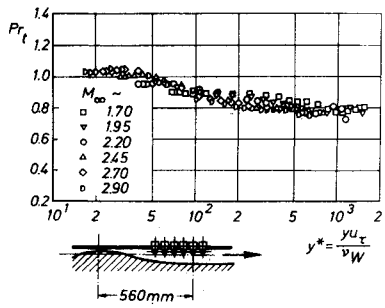

Fig. 10 Turbulent Prandtl numbers Pr_t vs dimensionless wall distance y^* on a flat nozzle wall.

values of Pr_t indicate an increase greater than unity for $y^* \leq 50$. This means that the turbulent transport of heat decreases more rapidly towards the wall than the momentum transport. The turbulent Prandtl number distributions obtained from measurements on the plane nozzle wall at nearly adiabatic conditions, show the same trend (Fig. 10).

The agreement between these results and those found by H. Ludwieg[9] from measurements in a pipe at high subsonic speeds, is good. These measurements also show the tendency of the turbulent Prandtl number to increase towards the wall. However, data points were available only for wall distances $y/\delta \geq 0.1$ and, therefore, no comparison can be made for the viscous layer.

The results of turbulent Prandtl number distributions for supersonic flow are in excellent agreement with those of R. L. Simpson, D. G. Whitten, and R. J. Moffat,[10] who carried out measurements at low subsonic speeds on a porous plate.

6. Approximate Calculation of the Total Temperature Distributions Near the Wall

A theoretical approach will confirm the previous results and, in addition, will shed some light on the mechanism of turbulent heat transport in the region close to the surface, where no measurements can be made. At sufficiently small distances y from the wall, all the derivatives of the mean quantities with respect to the x direction can be neglected in the governing differential equations. Integration of the equations for momentum and thermal energy Eqs. (9) and (10) thus yields the following relations for the shear stress and heat flux

$$\tau = \text{const} = \tau_W \tag{34}$$

$$q = q_W - U\tau_W \tag{35}$$

Within the region where these suppositions hold the distributions of Mach number and total temperature can be given as (compare Ref. 6)

$$M = M_\tau f(y^*, M_\tau, \beta_q) \tag{36}$$

$$T_0 = T_W \varphi(y^*, M_\tau, \beta_q) \tag{37}$$

where f and φ are dimensionless functions of y^*, the Mach number parameter M_τ, and the heat flux parameter β_q. These relations imply

$$T_0 = T_W F(M/M_\tau, M_\tau, \beta_q) \tag{38}$$

where F is another dimensionless function. The functions can be calculated from Eqs. (34) and (35), when simple flow models are introduced for τ and q. Using the mixing length conception, we have

$$\tau = \left(\mu + \rho l^2 \left|\frac{\partial U}{\partial y}\right|\right)\frac{\partial U}{\partial y} \tag{39}$$

and

$$q = c_p \left(\mu/Pr + \rho l^2 \left|\frac{\partial U}{\partial y}\right| Pr_t\right)\frac{\partial T}{\partial y} \tag{40}$$

where E. R. van Driest's relation[11] can be applied in the form (Ref. 6)

$$l = \varkappa y[1 - \exp\{-y(\tau_W \rho)^{1/2}/(\mu A)\}] \tag{41}$$

$\varkappa$ is von Kármán's constant and A is van Driest's constant. The assumption of a constant value of the turbulent Prandtl number is simple and suggests itself. However, the results, as calculated with a constant Pr_t, cannot be reconciled with the experimentally determined temperature distributions. For this reason, a different mixing length variation for the transport of heat, namely

$$l_q = l(Pr_t)^{-1/2} = \varkappa_q y\left[1 - \exp\left(\frac{-y(\tau_W \rho)^{1/2}}{\mu A_q}\right)\right] \tag{42}$$

is proposed as a generalization, which differs from Eq. (41) in that $\varkappa_q$ and A_q differ from $\varkappa$ and A, respectively. Equation (41) was originally suggested from an analogy with Stokes' flow on an oscillating wall. Although this analogy is not pertinent, the formula works well. Similar arguments may be advanced in favor of Eq. (42), but the assumptions can be justified only by comparison with experimental results. The following limiting relations hold

$$y = 0: \quad Pr_t = [(\varkappa/\varkappa_q)(A_q/A)]^2 \tag{43}$$

$$\lim y \to \infty: \quad Pr_t = (\varkappa/\varkappa_q)^2 \tag{44}$$

Some typical results, as calculated from numerical integration of Eqs. (34–42), are presented in the form of Eq. (38) together with experimental data at $M_\infty \sim 3$ ($M_\tau = 0.081$, $\beta_q = -0.0011$), on Fig. 11. There are two curves for $Pr_t = \text{const}$ ($A_q = A$) and one for laminar flow ($Pr = 0.72$). It becomes clear from these results that none of the possible curves with $Pr_t = \text{const}$ conforms to the experiments. However, the curve based on the values $(\varkappa/\varkappa_q)^2 = 0.86$, $A_q/A = 1.25$, comes close to the measured distribution. In this case, the turbulent Prandtl number varies from $Pr_t = 1.34$ at the surface to $Pr_t = 0.86$ in the fully turbulent part. At first glance, the shape of this temperature distribution appears to be surprising. But, at very small distances, the temperature and Mach number distributions are given by the laws of laminar flow (up to $M/M_\tau \sim 6$), and in order to join the measurements at larger M/M_τ, the temperature distribution has to assume the peculiarly crooked form. This form can be established only with a relatively low eddy heat conductivity, i.e. with a high turbulent Prandtl number in the viscous regime.

A quantitative comparison for measurements on the flat plate at several Mach numbers, ranging from $M_\infty = 2.5$ to

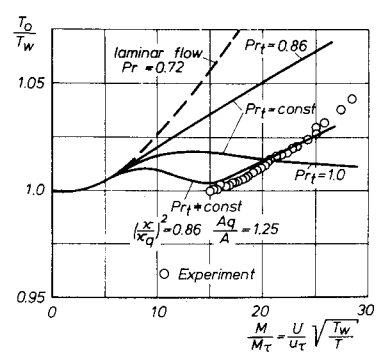

Fig. 11 Calculated total temperature distributions $M_\tau = 0.081$, $\beta_q = -0.0011$.

4.5, is shown on Fig. 12. The rate of heat transfer at the wall was estimated from Eqs. (27) and (29), using a recovery factor $r = 0.89$. For all the calculated curves the same set of constants was chosen, namely $(\varkappa/\varkappa_q)^2 = 0.86$, $A_q/A = 1.25$. Since the calculated values of q_W are very sensitive to the estimated difference $T_W - T_e$, two limiting curves were drawn in, assuming deviations from the measured surface temperature of $\pm 1°C$ and from the recovery factor of ∓ 0.01. The calculations agree well with the experiments, and the limiting curves envelop all the data. There is some indication that the ratios of the constants may have universal character. This is confirmed by inspection of the temperature measurements in boundary layers made by Adcock et al.[12] and Lee et al.[13] Finally, the parallel shift of the data below the calculated curve with $Pr_t = 0.86$, which follows from Fig. 11, was observed also for the previous comparisons (Ref. 6) with the early NOL-measurements.

A rigorous theory is not available for the turbulent flow, but we know that the pressure fluctuations provide the driving forces of the motion in the viscous sublayer. This follows from the work of J. Sternberg,[14] G. Schubert, and G. M. Corcos.[15] The absence of an equivalent term in the thermal energy equation may explain why the turbulent transport of heat decreases faster towards the wall than the turbulent transport of momentum.

Finally it may be mentioned that R. Jenkins[16] (compare also Ref. 10) proposed a model to predict the unequal variation of momentum and heat transport, when the ratio of eddy viscosity to kinematic viscosity ϵ_τ/ν decreases. We shall not discuss the details of this model here, but merely show, Fig. 13, that it predicts a similar variation of Pr_t with ϵ_τ/ν as our mixing length model.

7. Concluding Remarks

The measurements of total temperature distributions in the boundary layers of two wind tunnels are found in good agreement with each other in layers close to the surface. This follows from the turbulent Prandtl numbers, which were calculated from the data. The reason is that velocity as well as temperature distributions are governed by local wall parameters, such as shear stress τ_W, temperature T_W, rate of heat transfer q_W, pressure p_W, and gas properties. The data are obviously compatible with the similarity relations, derived from these parameters. Calculations based on the mixing length concept predict well velocity and temperature distributions from the surface through the viscous layer to the fully turbulent regime.

In contrast to this, the temperature distributions in the outer part of the boundary layers do not agree due to the different flow conditions of the two experiments. Actually, upstream history effects decay very slowly. The measurements on the plane nozzle wall agree qualitatively with the expected behavior. The circumstances which generate the observed temperature distributions on the flat plate, are not yet understood.

Further work is necessary to clarify apparent discrepancies. Direct surface shear stress measurements will be helfpul. Comparative profile measurements with the use of different kinds of temperature probes could be made. Experiments with severe rates of heat transfer would usefully supplement the present work on nearly adiabatic wall conditions.

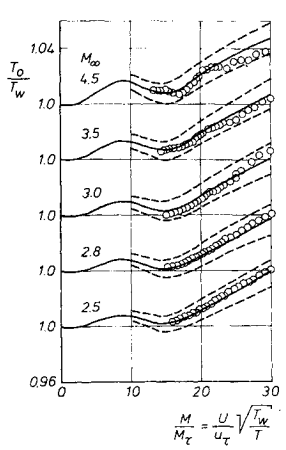

M_∞	$M_\tau \times 10^3$	$\beta_q \times 10^3$
4.5	104	-1.6 ± 0.7
3.5	89	-1.1 ± 0.6
3.0	81	-1.1 ± 0.6
2.8	77	-1.2 ± 0.6
2.5	71	-0.9 ± 0.5

Fig. 12 Calculated total temperature distributions compared with experimental results at different Mach numbers $(\varkappa, \varkappa_q)^2 = 0.86$, $A_q/A = 1.25$.

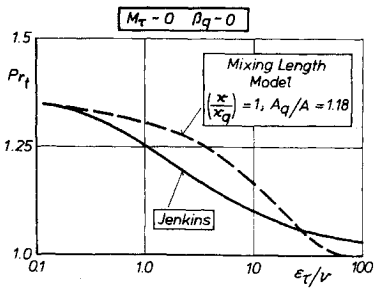

Fig. 13 Variation of the turbulent Prandtl number according to the mixing length and Jenkins' model.

References

[1] Rotta, J. C., "Heat Transfer and Temperature Distribution in Turbulent Boundary Layers at Supersonic and Hypersonic Flows," AGARDograph 97, 1965, pp. 35–63.

[2] Meier, H. U., "A Combined Temperature and Pressure Probe for Compressible Flow," *AIAA Journal*, Vol. 7, No. 3, March 1969, pp. 529–530.

[3] Hastings, R. C. and Sawyer, W. G., "Turbulent Boundary Layer on a Large Flat Plate at $M = 4$," RAE TR 70040, 1970, Royal Aircraft Establishment, Bedford.

[4] Mabey, D. G., Sawyer, W. G., and Meier, H. U., "Boundary Layer Measurements on a Flat Plate at Mach Numbers from 2.5 to 4.5 with Theoretical Comparisons (Part I)," RAE TR, Royal Aircraft Establishment, Bedford (in preparation).

[5] Meier, H. U., "Messungen von turbulenten Grenzschichten an einer wärmeisolierten Wand im kleinen Ueberschallwindkanal der AVA," *Zeitschrift für Flugwiss*, Vol. 17, No. 1, 1969, pp. 1–8; also available TT F-12 547, 1969, NASA.

[6] Rotta, J. C., "Ueber den Einfluß der Machschen Zahl und des Wärme-übergangs auf das Wandgesetz turbulenter Strömung," *Zeitschriftfür Flugwiss*, Vol. 7, No. 9, 1959, pp. 264–274.

[7] Meier, H. U., "Experimentelle und theoretische Untersuchungen von turbulenten Grenzschichten bei Ueberschallströmung," Mitteilungen aus dem Max-Planck-Institut für Strömungsforschung und der Aerodynamischen Versuchsanstalt Göttingen, No. 49, 1970, pp. 1–112.

[8] Schlichting, H., *Boundary Layer Theory*, 6th ed., McGraw-Hill, New York, 1968.

[9] Ludwieg, H., "Bestimmung des Verhältnisses der Austauschkoeffizienten für Wärme und Impuls bei turbulenten Grenzschichten," *Zeitschrift für Flugwiss*, Vol. 4, No. 1/2, 1956, pp. 73–81.

[10] Simpson, R. L., Whitten, D. G., and Moffat, R. J., "An Experimental Study of the Turbulent Prandtl Number of Air with Injection and Suction," *International Journal of Heat Mass Transfer*, Vol. 13, 1970, pp. 125–143.

[11] van Driest, E. R., "On Turbulent Flow Near a Wall," *Journal of the Aeronautical Sciences*, Vol. 23, 1956, pp. 1007–1011.

[12] Adcock, J. B., Peterson, J. B., Jr., and McRee, D. L., "Experimental Investigations of a Turbulent Boundary Layer at Mach 6, High Reynolds Numbers, and Zero Heat Transfer," TN D 2907, 1965, NASA.

[13] Lee, R. E., Yanta, W. J., and Leonas, A. C., "Velocity Profile, Skin Friction Balance and Heat Transfer Measurements of the Turbulent Boundary Layer at Mach 5," *Proceedings of the*

1968 Heat Transfer Fluid Mechanics Institute, Stanford University Press, pp. 3–17.

[14] Sternberg, J., "A Theory for the Viscous Sublayer of a Turbulent Flow," *Journal of Fluid Mechanics*, Vol. 13, 1962, pp. 241–271.

[15] Schubert, G. and Corcos, G. M., "The Dynamics of Turbulence Near a Wall According to a Linear Model," *Journal of Fluid Mechanics*, Vol. 29, 1967, pp. 113–135.

[16] Jenkins, R., "Variation of the Eddy Conductivity with Prandtl Modulus and its Use in Prediction of Turbulent Heat Transfer," Heat Transfer and Fluid Mechanics Institute, Stanford University Press, 1951, pp. 147–158.

NOVEMBER 1971 AIAA JOURNAL VOL. 9, NO. 11

Parametric Study of a Two-Dimensional Turbulent Wall Jet in a Moving Stream with Arbitrary Pressure Gradient

SURESH H. GORADIA* AND GENE T. COLWELL†
Georgia Institute of Technology, Atlanta, Ga.

Measurements of flow parameters for a two-dimensional turbulent wall jet are presented in a range of ratios of slot stream velocity to external stream velocity with pressure gradients, not previously investigated. These data are utilized for the calculations of wall shear and shear distribution by numerical methods. Relationships among the parameters are considered.

Nomenclature

C_p = pressure coefficient
$f(\eta_1)$ = similarity function for velocity profile in the jet layer in initial region
$f(\eta_2)$ = similarity function for velocity profile in the wake layer in the initial region
$f(\eta_3)$ = similarity function for velocity profile in the jet layer in main region
$f(\eta_4)$ = similarity function for velocity profile in the wake layer in the main region
H = form factor or pressure gradient parameter
$\tilde{H}$ = ratio of dissipation energy thickness and momentum thickness
M = Mach number
P_{ST} = wall static pressure, lbf/ft²
P_T = Pitot tube total pressure, lbf/ft²
P_∞ = freestream pressure lbf/ft²
$R_{e\theta}$ = Reynolds number based on wall layer momentum thickness
U_c = velocity in the core layer in the initial region, fps
$U_{c(0)}$ = slot velocity at the exit, fps
$U_{e(x)}$ = velocity at the edge of viscous layer, fps
$U_{e(0)}$ = velocity at the edge of viscous layer at the slot exit, fps
$U_{w(x)}$ = velocity at the junction of jet layer and wake layer, fps
$U_{m(x)}$ = velocity at the junction of wall layer and jet layer, fps
U_∞ = freestream velocity, fps
u = X component of velocity in viscous layer, fps
v = Y component of velocity in viscous layer, fps
x = distance measured from slot exit, in.
y = distance measured from wall, in.
y_{1c} = distance y in the wake layer above the wall in initial region for $f(\eta_2) = 0.5$, in.
y_{2c} = distance y in the wake layer above the wall in main region for $f(\eta_4) = 0.5$, in.
δ^* = displacement thickness for wall layer in initial and main region, in. $\int_0^{\delta_1} [1 - (u/U_c)]dy$ or $\int_0^{\delta_5} [1 - (u/U_m)]dy$
δ^{**} = dissipation energy thickness, in. $\int_0^{\delta_1} (u/U_c)[1 - (u/U_c)^2]\,dy$ or $\int_0^{\delta_5} (u/U_m)[1 - (u/U_m)^2]\,dy$
$\delta_1, \delta_2, \delta_3, \delta_4, \delta_5$, etc. = distance shown in Fig. 1, in.
η_1 = similarity parameter for velocity profile in the jet layer in the initial region
η_2 = similarity parameter for velocity profile in the wake layer in the initial region
η_3 = similarity parameter for velocity profile in the jet layer in the main region
η_4 = similarity parameter for velocity profile in the wake layer in the main region
θ = momentum thickness for wall layer in initial region and main region, in. $\int_0^{\delta_1} (u/U_c)[1 - (u/U_c)]dy$ or $\int_0^{\delta_5} (u/U_m)[1 - (u/U_m)]dy$
ρ = density of air, lbm/ft³
τ = shear stress at a distance y above wall, lbf/ft²
τ_w = wall shear stress, lbf/ft²

Received November 11, 1970; revision received May 17, 1971. Considerable credit is due Y. T. Chin and R. F. Tanner of Lockheed Georgia Company, who originally built the majority of the test rig that was used during the course of these experiments. Also, much credit is due T. Dansby, D. M. Ryle, and B. H. Little of Lockheed Georgia Company for their support and advice.

Index category: Boundary Layers and Convective Heat Transfer–Turbulent.

* Graduate Student, School of Mechanical Engineering; also Senior Aerodynamic Engineer, Lockheed Georgia Company, Marietta, Ga.

† Associate Professor, School of Mechanical Engineering.

Introduction

THE behavior of wall jets is of practical interest because of their application in film cooling or heating and in boundary-layer control on airfoil sections and wings of STOL aircraft. Detailed experimental investigations have been carried out by prominent investigators such as Bradshaw and Gee,[1] Kruka and Eskinazi,[2] Myers et al.,[3] Hubbart and Bangart,[4] Birkebak et al.,[5] and Kacker and Whitelaw.[6] Some of the investigators concentrated their efforts on very